Published in final edited form as:

IEEE Trans Radiat Plasma Med Sci. 2019 January ; 3(1): 31–37. doi:10.1109/trpms.2018.2842463.

Development of a Customizable Hepatic Arterial Tree and Particle Transport Model for Use in Treatment Planning

Nathan R. Crookston [graduate student in Computer Engineering],
Johns Hopkins University, Baltimore, MD 21218 (ncrooks1@jhu.edu).

George S. K. Fung,
Department of Medical Imaging Physics, Johns Hopkins Medicine, Baltimore, MD 21287 (gskfung@jhmi.edu).

Eric C. Frey
Department of Medical Imaging Physics, Johns Hopkins Medicine, Baltimore, MD 21287 (efrey@jhmi.edu).

Abstract

Optimal treatment planning for radioembolization of hepatic cancers produces sufficient dose to tumors for control and dose to normal liver parenchyma that is below the threshold for toxicity. The non-uniform distribution of particles in liver microanatomy complicates the planning process as different functional regions receive different doses. Having realistic and patient-specific models of the arterial tree and microsphere trapping would be useful for developing more optimal treatment plans. We propose a macrocell-based growth method to generate models of the hepatic arterial tree from the proper hepatic artery to the terminal arterioles supplying the capillaries in the parenchyma. We show how these trees can be adapted to match patient values of pressure, flow, and vessel diameters while still conforming to laws controlling vessel bifurcation, changes in pressure, and blood flow. We also introduce a method to model particle transport within the tree that accounts for vessel and particle diameter distributions and show the non-uniform microsphere deposition pattern that results. Potential applications include investigating dose heterogeneity and microsphere deposition patterns.

Keywords

dosimetry; liver radioembolization; particle transport; treatment planning; vascular modeling

I. Introduction

THE use of radioembolization (RE) for treating metastatic and primary liver cancers is increasing due to its ability to deliver high treatment doses to tumor tissue and low doses to normal liver parenchyma, thus reducing liver toxicity compared to external beam radiotherapy [1]. Treatment is performed by inserting a catheter into the hepatic artery and administering radioactive microspheres that embolize the microvasculature and deliver radiation near the location of embolization. Due to the tumors' primary use of arterial blood [1], particles are likely to be trapped near and deliver a high absorbed dose to tumors while sparing normal liver structures.

other approaches, such as fractionated external beam radiation therapy, induce toxicity at much lower doses than RE, and this may not allow a fatal dose of radiation to be delivered to tumors [2]. Optimal treatment plans for RE must deliver sufficient dose for tumor control while avoiding complications such as radiation-induced liver disease due to excessive dose to normal tissues. Treatment planning for RE using glass microspheres principally uses the total mass of the treated liver volume to calculate the mean dose [3]. This planning method aims to deliver a desired average dose to the treated volume and does not account for tumor burden, the ratio of microspheres trapped in tumors versus normal tissues, and their effects on dose heterogeneity. Thus, dose delivered to tumors varies across patients, and this can result in a lower probability of tumor control due to under-dosing of the tumor [4]. The calculation of dose to normal liver tissue is complicated by the non-uniform distribution of microspheres within that tissue and the unique microstructure of the liver itself [5].

Because of the relatively short range of the Y-90 beta particles and their nonuniform distribution in the anatomy, it has recently been suggested that the dose at a microscopic level is highly non-uniform, and that this affects the radiation toxicity of normal tissues [5]. Accurately predicting the dose to normal liver tissue at a microscopic level through modeling of patients' liver microanatomies could allow dose adjustment and improve the outcomes of patient treatment. In order to effectively model particle distribution within a given patient's vasculature, a realistic model of that vasculature is required. However, at present there is no method to map the microvasculature *in vivo*. Also, there are differences in the distribution of particle diameters that may affect the final trapping locations of spheres within the microvasculature. The details of this trapping depend, in principle, on details of the vessel diameters, blood pressure, and mechanism of trapping.

Bézy-Wendling *et al.* proposed a method to create a realistic representation of hepatic vasculature based on measured physical properties and an optimality criterion that minimized local vessel volume [6]. The method uses macrocells to incrementally extend an initial vascular tree to perfuse an existing liver shape. The vessels in the generated tree split and taper realistically after each bifurcation from the proper hepatic artery (PHA) to the macrocell connection points.

In their work, however, vessels were generated down to regions two hundred times larger than the size of a macrocell representing a terminal arteriole [7]. At this scale, the terminal vessel diameters are larger than the average diameter of the infused microspheres in RE [8]. Also, without generating vessels down to dimensions of the terminal hepatic arteriole (THA) diameters, it is difficult to check the validity of the tree generation method as most data have been collected for initial and terminal vessels. Also, if the vessel diameters in the resulting vascular tree model are larger than the sizes of the infused particles, the tree will not be useful for modeling the trapping of microspheres at a microanatomical scale.

Walrand *et al.* have developed a model of the liver microanatomy, the hepatic arterial tree, and the microsphere infusion process for high-activity, glass microspheres [5] [9]. The tree was generated using an initial hepatic arterial tree supplying the eight liver segments. Those segments were filled with hexagonal prisms that represent the lobule, a functional unit of the liver with blood flowing in at each corner through portal tracts containing one or more THAs

and portal venules [10]. To generate a tree from the THAs, each arteriole was chosen at random and connected to the nearest existing vessel that would not result in retrograde flow. Blood flow in each vessel was determined based on the number of terminal arterioles supplied by the vessel or its descendants. This model did not estimate the diameters of any intervening vessels nor take into account blood flow or pressure differentials when generating the tree.

Walrand's particle trapping model assumed that all particles are trapped in THAs and that particle flow at bifurcations is probabilistic and based on both flow and the relative geometry of the child vessels. Simulated images of the activity distribution after a simulated RE procedure had a texture that was qualitatively similar to that observed in PET/CT images.

However, the tree produced by this method does not follow observed physical properties. This may impact the heterogeneity of particle and dose distribution. Additionally, the assumption that each particle arrives at a terminal arteriole is unlikely given the range of diameters of microspheres [3] and the measured diameters of the arterioles [11]. Högberg has demonstrated that resin microspheres, which have diameters similar to glass microspheres, are frequently trapped in nonterminal vessels [12].

In this work, we propose a method to generate a vascular tree using a liver volume and the larger branches of the hepatic arterial tree that can be estimated from patient scans. The simulated tree conforms to relevant physical laws and can be adapted to match measured pressure differentials, blood flows, viscosities, and vessel diameters. The blood flow patterns and pressures can be customized for individual patients; e.g., using data from patient scans or measured via a catheter. We also propose a new method to model the infusion and trapping of embolizing particles in those trees that considers the diameters of both the particles and trapping vessels. These can be used to produce estimates of the particle distribution that could be useful for exploring the microscopic dose distribution in normal liver tissues and predict normal tissue dose on an individualized basis.

II. Methods

In this work, we have developed a method to generate a hepatic arterial tree from the PHA to individual THAs. This method uses the macrocell-growth algorithm described by Bézy-Wendling *et al.* [6]; various model parameters are adjusted dynamically during tree growth to produce desired quantities of interest such as THA diameters. As will be described below, the binary trees generated using this method conserve matter, conform to Murray's law at all bifurcations, and follow Poiseuille's law within each vessel.

A. Conservation of Matter

To conserve matter, the volume of blood flowing into each vessel equals the volume flowing out of its children, or

$$Q_p = Q_{c1} + Q_{c2}, \tag{1}$$

where Q_p and Q_{c_x} are the volume flow of blood, modeled as an incompressible fluid, passing through the parent and child vessels. At the highest level, the flow from the PHA equals the total volume of blood flowing out of all terminal arterioles. In this work, we chose to have equal flow to each terminal arteriole, though non-uniform flow distributions could be incorporated if there was knowledge of local relative flow, e.g., from perfusion imaging.

B. Murray's Law

Murray's law describes the relationship between the diameters of a parent vessel and its child vessels [13]. For binary trees, it may be expressed as $r_p^\gamma = r_{c1}^\gamma + r_{c2}^\gamma$, where r_p is the radius of the parent vessel, r_{cx} is the radius of each child vessel, and γ is the bifurcation constant. Murray originally suggested $\gamma = 3$ to minimize the power necessary to provide adequate blood flow [14], but it is generally accepted that γ varies, depending on the type and caliber of the vessels, from 2 in larger arteries near the heart to 3 in smaller vessels [15].

We have chosen γ based on the vessel diameter ratio (VDR), i.e., the ratio of the diameter of the PHA (4.5 mm [16]) and the average THA diameter (11.8 μm [11]). For a balanced binary tree with equal child vessel diameters, the relation between the parent and child vessels may be expressed as a scalar

$$r_p = 2^{\frac{1}{\gamma}} \cdot r_c \,. \tag{2}$$

For a balanced tree with n levels of branching, the VDR is expressed as

$$VDR = \frac{r_{PHA}}{r_{THA}} = 2^{\frac{n}{\gamma}} \,. \tag{3}$$

The value of n may be estimated for a balanced binary tree with the expression $\log_2$ (*number of THAs*). The number of THAs can either be determined by filling the liver segmentation with THAs or be estimated by dividing the volume of the liver by the volume of a lobule ($1.87 \cdot 10^{-3}$mL) and multiplying by two, as the six portal tracts of a lobule are shared by three other lobules. Thus, an expression to calculate the bifurcation constant for a balanced binary tree, given vessel diameters and the number of THAs, is

$$\gamma = \frac{\log_2 (number\ of\ THAs)}{\log_2 r_{PHA} - \log_2 r_{THA}} \,. \tag{4}$$

Trees generated in this work were unbalanced, which affects both n and γ. The error caused by using (4) for unbalanced trees was assessed by observing the percent differences in VDR for trees generated with values of γ between 2 and 3.

C. Poiseuille's Law

Poiseuille's law [6] gives the pressure differential (ΔP) between the extremes of a cylinder as a function of the length (l) and radius (r) of that cylinder, and the viscosity (μ) and volume flow rate (Q) of a Newtonian fluid in that cylinder:

$$\Delta P = 8Q\frac{\mu l}{\pi r^4}.$$

While blood is not a Newtonian fluid [17], and arterial flow is not laminar [14] [15], Poiseuille's law is still commonly used to model physical parameters of individual vessels [6] [15].

The choice of Murray's bifurcation constant controls the VDR, but the generated vessel diameters depend on l, μ, ΔP, and Q. The values of these parameters used in this work are justified below.

The length, l, of a particular vessel is not directly controllable using the macrocell-based generation method. Instead, it is dependent on the locations of the PHA and macrocells and on the optimization criteria used to determine vessel bifurcation points, as discussed below.

The viscosity, μ, of blood depends on factors such as the hematocrit, plasma content, and vessel diameter [17]. Bézy-Wendling *et al.* argued that treating blood viscosity as a constant is a reasonable first approximation [6]. Thus, the effects of modeling blood as a non-Newtonian fluid were not considered in this work; we approximated blood as a fluid with constant viscosity of 3.5 mPa·s [18].

A wide range of pressures in the PHA and THAs has been measured across populations and within individuals [19] [20] [10]. In this work, we typically used 98 mmHg as the pressure at the input of the PHA [21] and 25 mmHg as the output pressure at each THA [10].

The flow of arterial blood, Q, is also highly variable [22] and depends on both the input blood pressure and the flow within the portal vein [19]. Unless otherwise noted, we adjusted the arterial blood flow to produce an average THA diameter consistent with that reported in the literature.

D. Tree Generation

Vessel trees were generated using the macrocell-based approach described by Bézy-Wendling [6] and Kretowski [21] that simulates the growth of the liver and its vascular tree over a series of 15 cycles. The macrocells represent THAs whose locations are the corners of hexagonal prisms arranged in a lattice as described in the virtual arterial tree by Walrand *et al.* [9]. The growth process starts with an initial segmentation of the hepatic artery and the liver shape. In the work presented here, the liver shape was taken from the XCAT phantom [23] and has volume 1.75 L. The initial hepatic arterial tree was also taken from the XCAT and has 3 branching levels. Both could instead be segmented from patient images. The liver shape is filled with lobules as done for the virtual arterial tree in Walrand *et al.* [9], and the THA locations in the lobules are stored as the potential macrocell locations. The initial tree, liver shape, and macrocell locations are then scaled to one-twentieth of the final model volume. Active macrocell locations are chosen such that the number of macrocells per unit volume is the same for all cycles without being too close together. For the first cycle, then, one-twentieth of the macrocell locations are designated as active and unoccupied for the

current cycle. During that cycle, those macrocell locations are occupied through the proliferation of macrocells over a series of subcycles.

During a subcycle, each macrocell has some probability of mitosis (dividing) and apoptosis (dying), as shown in figure 1. At the start of each cycle, every macrocell is tested to determine if it will divide, die, or remain unchanged. A new macrocell is generated for each dividing macrocell, and the new macrocell occupies a nearby, active location, if available, and is connected via a new vessel to the nearest branch of the existing hepatic arterial tree. The connection point is controlled by physical principles that optimize the flow of blood through those vessels and is discussed below. If there are no nearby unoccupied, active locations, then the new macrocell is removed. The order in which new macrocells are processed is random. When a macrocell is marked for deletion, the vessels connecting it to the tree are removed and flow values in parent vessels are recalculated. The process of mitosis and apoptosis in subcycles continues until the cycle termination criterion is reached. The termination criterion is that more macrocells die than are created in a subcycle, which indicates that nearly all active macrocell locations are occupied. At that point, the current cycle is ended, and the liver volume, hepatic arterial tree, and potential macrocell locations are scaled up linearly to fill a larger liver volume. A superset of potential macrocell locations are identified as before, and a new set of subcycles begins until the cycle termination criterion is reached. These cycles continue until the liver matches its original volume.

During later cycles, when the number of vessels is in the tens of millions, searching for the nearest vessel to a proposed THA location can take a significant amount of time. This was mitigated by storing vessel locations in an octree data structure [24], reducing the complexity of searching from linear to logarithmic.

When macrocells are added to the model, the nearest vessel is bifurcated to supply blood to both the new macrocell and the vessel's previous perfusion area. When this occurs, an optimality criterion determines the location of the bifurcation point [6]. Zamir *et al.* investigated several optimality criteria, including minimizing the power to pump blood through a junction, and minimizing vessel surface area, volume, or shear stress at a junction [25]. However, there is not consensus on which optimality criterion is most physiologically realistic [26]. Bézy-Wendling *et al.* chose to minimize local vessel volume to determine the optimal bifurcation point [6], which minimizes the amount of blood required to perfuse the organ and the time it takes for blood-born items to circulate [26]. Fung *et al.* chose to minimize the shear stress on vessel walls [27], which has the benefit of determining the bifurcation point based solely on information available to each locally growing vessel [26]. The derivation in [27] supplies a formula for choosing the optimal point for a bifurcation that depends only on the vessel endpoints and the relative flow in each vessel. This reduces the computational effort necessary to choose bifurcation points. Due to the large number of vessels being generated in this work, we minimize the shear stress on vessel walls as described by Fung.

During tree growth, the vessel diameters, pressures, and flow rates are periodically computed as described by Kretowski *et al.* [21]. In this method, vessel diameter is the dependent variable and the change in pressure, blood flow, and vessel length are independent

variables. Using this method to generate a tree with correct THA diameters requires that the flow (or other variable) be adjusted after construction is finished. The flows are adjusted as follows: After the tree is generated and K macrocells perfused, there is one path from the PHA to each macrocell. For each path, we can write

$$\Delta P_{ALL} = P_{PHA} - P_{THA} = \sum_{i=1}^{n_x} \frac{8 Q_{x_i} \mu l_{x_i}}{\pi r_{x_i}^4}, \tag{5}$$

where n_x is the number of vessels in path x, and Q_{x_i}, l_{x_i} and r_{x_i} are the flow, length, and radius of the ith segment of path x. Here we wish to change the total hepatic flow, Q, to achieve a particular average THA diameter without changing any other parameters. Due to (1), scaling Q by a factor results in each Q_{x_i} being scaled by the same factor. The result for each r_{x_i} is complicated by the non-linear constraint imposed by Murray's law. If we use the same assumption used in (2) and (3), we can rewrite (5) in terms of r_{THA}, the average terminal radius, as

$$\Delta P_{ALL} = \sum_{i=1}^{n_x} \frac{8 Q_{x_i} \mu l_{x_i}}{\pi 2^{4(i-1)/\gamma} \cdot r_{THA}^4}, \tag{6}$$

Equation (6) remains balanced if, for any scalar α applied to r_{THA}, each Q_{x_i} (and by extension, Q) is scaled by α^4. The validity of the simplification was tested by comparing the average THA diameter for different Q and ΔP_{ALL} with the predicted diameters, as described below.

E. Trapping Model

In addition to a model of the hepatic arterial tree, we have adapted the particle trapping model developed by Walrand *et al.* to take into account the diameter-distribution of the particles and the diameters of the vessels. The modified algorithm operates by randomly sampling a diameter from the particle diameter-distribution and placing a particle of that size into the initial vessel of the tree. The particle then flows through the tree until it arrives at a vessel that is either too narrow for the particle or is a terminal arteriole. At each bifurcation, the particle randomly enters the left or right child vessel, depending on the vessels' geometries at the bifurcation and the division of blood flow, as described by Walrand [9]. The particle is trapped if both vessels are smaller than the particle diameter, but, if only one vessel is too small, the particle enters the larger vessel. We simulated the effect of embolization by linearly reducing flow through a vessel, in proportion to the number of particles trapped in it, until 50 particles are trapped and flow to that vessel stops. After a particle is trapped and the flow in the vessel adjusted, the flow and bifurcation probabilities are recalculated for the whole tree.

Several 120 Gy whole-liver infusions were modeled for trees generated as described above with average THAs of 11.8 μm. Further 120 Gy infusions were simulated for trees with average THA diameters of 15.8 μm and 18.3 μm to compare the fraction of infused spheres arriving at THAs. All infusions were modeled with particles simulating glass microspheres

whose diameter distribution was a truncated Gaussian with mean 25 μm and standard deviation 5 μm [2].

III. Results

Estimating the bifurcation constant that produces the correct VDR using (4) with 1,868,346 THAs (estimated using liver volume), yielded $\gamma = 2.43$. Trees generated using this method had an average of 1,849,429 macrocells, and each terminal arteriole perfusing a macrocell had, on average, 435 bifurcations between itself and the PHA, which is much larger than the 21 bifurcations necessary for a balanced tree. Figure 2 shows that the relative differences between the expected VDRs for balanced trees and the VDRs for generated trees was between 2% and 8% for a range of bifurcation constants. This indicates that (4) is a reasonable means to estimate the bifurcation constant, despite the asymmetry of the vessel tree.

Figures 3 and 4 show the relationship between the average THA diameter and blood flow and pressure differential. Each figure shows the relative error between the actual average THA diameter and the diameter predicted for a balanced tree. In both cases, the error was much less than 1% of the predicted value. This indicates that approximating the relationship between parent and children vessels as a simple scalar, as in (2) and (6), does not have a significant effect on the relationship between flow, pressure, and the THA diameters. It was thus possible to directly calculate the flow required to produce a tree matching the desired average THA diameter.

Figure 5 illustrates the growth of the vessel tree from the initial hepatic artery segmentation to the full-grown tree with γ 2.428, $Q = 75$ mL/min, and $\Delta P = 73$ mmHg. At each cycle, the pressure, flow, and diameters were optimized as described above to create a realistic tree whose vessels taper with successive generations and for which blood flows with minimal drag. The generated tree had a PHA diameter of 4.63 mm and a mean THA diameter of 11.79 μm with a standard deviation of 2.45 μm.

After sphere distribution, a volume image with 2 mm pixel widths was generated. That image was then convolved with a 3-dimensional Gaussian filter with FWHM 8 mm to create an image with resolution similar to that of Y-90 PET. A single coronal slice from near the center of the volume was extracted and is displayed as figure 6.

A very small percentage of particles arrived in the THAs for any average THA diameter tested in this work. Trees with 75 mL/min total flow and 11.8 μm average THA diameter trapped 0.087% of infused microspheres. For trees with 241 mL/min flow and 15.8 μm diameters, the percentage increased to 0.103%. Trees with 433 mL/min flow and 18.3 μm average THA diameters had 0.116% of microspheres trapped in THAs.

IV. Discussion

The relatively small errors between the predicted and observed VDRs indicates that, at least for minimum drag bifurcation point optimization, the bifurcation constant can be estimated without knowing *a priori* how the tree will grow, or even how asymmetrical it will be.

Furthermore, we investigated the effect of modeling a different number of portal tracts on the value of γ needed to produce the desired THA diameter. We found that if each portal tract contains 2.4 THAs on average (as noted by Crawford [11]), a value $\gamma = 2.57$ was calculated, which is very close to the value measured in the coronary arteries of canines and that minimizes reflection at bifurcations with equal child flow [28].

Figures 3 and 4 show that (6) is a reasonable method to choose a value for flow or pressure difference that will produce a tree with the desired THA or PHA diameters. Together with Kretowski's original algorithm, this allows each generated tree to be customized with respect to the different parameters of interest such as pressure difference, blood flow volume, and average THA diameter.

In this work, we adjusted flow to produce terminal vessels with an average diameter matching literature values. However, the flow required for correct diameters, 75 mL/min, is lower than values reported in literature [19] [22]. If a Gaussian curve is representative of the data collected by Carlisle *et al.* [22], hepatic arterial flow of 75 mL/min or less would be representative of less than 3% of subjects measured. As our interest was in producing trees with reasonable THA diameters, we decided to use this value of flow. Further refinements to the flow model may help correct this apparent discrepancy, e.g., by modeling blood as a non-Newtonian fluid [14] or determining the value of the bifurcation constant at each junction in a more sophisticated manner.

The standard deviation of the generated THA diameters was only half as large as that reported by Crawford [11]. This resulted in many fewer terminal arterioles larger than 25 μm than was reported in that work. The simulations with larger THA diameters, despite having physically realistic values for flow and percentage of THAs with diameter greater than 25 μm, resulted in only slightly more particles being trapped in THAs. This is potentially important for predicting toxicity as the lobules contain physiologically important and radiosensitive structures critical for liver function [7], and microspheres trapped closer to them would deposit more dose in them. Nevertheless, the data show that the differences in the fraction of spheres trapped in THAs was less than 0.03% for the range of THA diameters investigated. The fact that so few spheres were trapped in THAs may be important as sphere trapping heterogeneity directly affects dose heterogeneity [5] [7] and may affect both tumor dose and toxicity to normal tissue.

Figure 6 shows a simulated SPECT image slice that would be obtained using an activity distribution generated using the models developed in this work. The non-uniform texture of the slice is qualitatively similar to the texture observed in patient images and those simulated by Walrand *et al.*

One potential application of the proposed method is the use of the diameter-aware particle trapping model described in this work to compare infusions of particles of different sizes. For example, the average diameter and standard deviation of macroaggregated albumin (MAA) particles are both larger than the same parameters for glass microspheres; differences in microsphere versus MAA distribution could be used to improve the accuracy of RE treatment plans based on measured MAA activity distributions.

The particle trapping model described here allows vessels to fill with particles and may cause them to divert to other branches or trap in a parent vessel. This yields more complex clusters than an algorithm that traps all particles in terminal arterioles, as was assumed in Walrand's original work [9]. A possible method to validate the proposed particle trapping model is to perform cluster analysis on the particle distribution and compare that with clusters observed in actual treated liver tissue. As clustering behavior may be very important to normal liver dose tolerance [7], producing realistic deposition patterns could allow trees generated using this method to be used in treatment planning. Activity distributions resulting from realistic clusters of spheres can also be used to test and validate image reconstruction methods targeting improved estimation of RE activity images.

Another potential improvement to this model is modifying the macrocells to represent hypervascularized and necrotic tissue in addition to normal parenchyma. Simulations with such tissue heterogeneity may capture important information about the tumor dose and normal tissue toxicity.

This model has potential applications in patient-specific treatment planning. In particular, the model of hepatic arterial vasculature can be made patient specific using imaging data in at least three ways. First, it can easily be adapted to the shape of the liver of a specific patient, obtained, e.g., from a CT image. Second, the initial vascular tree used to seed the vessel growth algorithm could be obtained from high resolution CT or MR angiography images. Finally, perfusion patterns measured via MR or CT imaging or flow or pressure measurements made using the catheter could potentially be used to constrain these parameters in the images. All of these together could provide a patient-specific model of the vasculature and, when combined with a model of particle trapping, be used to estimate dose distributions at a microscopic level. Combined with radiobiological models [5], this could provide patient-specific estimates of liver toxicity.

V. Summary

In this work, we have presented a new method for generating realistic models of the hepatic arterial tree using a macrocell growth technique. The generated tree conserves mass, satisfies Murray's law of vessel diameters at bifurcation points, and uses Poiseuille's law to calculate the pressure change through the vascular network. Physical parameters describing blood flow through the tree were based on literature values and modified to provide realistic average diameters for the terminal hepatic arterioles. A model for trapping particles with a known distribution of diameters was developed. The combination of these methods is useful for generating realistic activity distributions to validate image reconstruction methods and to explore the effect of various parameters, including differences in particle diameter distribution, on the microscopic dose distribution. The method allows for specification of the initial hepatic arterial tree, patient volume, and local variations in blood flow, providing future potential for improved patient-specific treatment planning.

References

[1]. Memon K et al., “Yttrium 90 Microspheres for the Treatment of Hepatocellular Carcinoma,” Multidisciplinary Treatment of Hepatocellular Carcinoma, Recent Results in Cancer Research, vol 190. Vauthey JN, Brouquet A, Ed. Springer, Berlin, Heidelberg, 2013, pp. 207–224

[2]. Dezarn WA, et al., "Recommendations of the American Association of Physicists in Medicine on dosimetry, imaging, and quality assurance procedures for 90Y microsphere brachytherapy in the treatment of hepatic malignancies." Medical physics, vol. 38 no. 8 pp. 4824–4845, 8. 2011. [PubMed: 21928655]

[3]. Therasphere USA Package Insert Rev. 14. Biocompatibles UK Ltd., a BTG International group company. [Online]. Available: https://www.btg-im.com/BTG/media/TheraSphere-Documents/PDF/TheraSphere-Package-Insert_USA_Rev-14.pdf, Accessed on: Dec. 19, 2017

[4]. Garin E, et al., "High impact of macroaggregated albumin-based tumour dose on response and overall survival in hepatocellular carcinoma patients treated with 90Y-loaded glass microsphere radioembolization." Liver International, vol. 37, no.1, pp. 101–110, 2017. [PubMed: 27514012]

[5]. Walrand S et al., “A hepatic dose-toxicity model opening the way toward individualized radioembolization planning.” J. Nucl. Med, vol. 55, no. 8, pp. 1317–1322, Aug. 2014. [PubMed: 24904111]

[6]. Bézy-Wendling J and Bruno A. "A 3D dynamic model of vascular trees." J. Biol. Syst, vol. 7, no. 1, pp. 11–31, 3 1999.

[7]. Gulec SA et al., “Hepatic structural dosimetry in 90Y microsphere treatment: a Monte Carlo modeling approach based on lobular microanatomy.” J. Nucl. Med, vol. 51, no. 2, pp. 301–310, 2. 2010. [PubMed: 20080888]

[8]. Kretowski M, et al., "Physiologically based modeling of 3-D vascular networks and CT scan angiography." IEEE transactions on medical imaging, vol. 22, no.2, pp. 248–257, 2. 2003. [PubMed: 12716001]

[9]. Walrand S et al., "The low hepatic toxicity per Gray of 90Y glass microspheres is linked to their transport in the arterial tree favoring a nonuniform trapping as observed in posttherapy PET imaging." J. Nucl. Med, vol. 55, no. 1, pp. 135–140, 1. 2014. [PubMed: 24296766]

[10]. Vollmar B, Menger MD, "The hepatic microcirculation: mechanistic contributions and therapeutic targets in liver injury and repair." Physiological reviews, vol. 89, no. 4, pp. 1269–1339, 10. 2009. [PubMed: 19789382]

[11]. Crawford AR, Lin X-Z, Crawford JM, “The normal adult human liver biopsy: A quantitative reference standard.” Hepatology, vol. 28, no. 2, pp. 323–331, 8. 1998. [PubMed: 9695993]

[12]. Högberg J, et al., "Increased absorbed liver dose in Selective Internal Radiation Therapy (SIRT) correlates with increased sphere-cluster frequency and absorbed dose inhomogeneity." EJNMMI physics, vol. 2, no.1, p. 10, 4 2015. [PubMed: 26501812]

[13]. Sherman TF, "On connecting large vessels to small. The meaning of Murray’s law." J. Gen. Physiology, vol. 78, no. 4, pp. 431–453, 10. 1981.

[14]. Revellin R, et al., "Extension of Murray's law using a non-Newtonian model of blood flow." Theoretical Biology and Medical Modelling, vol. 6, no.1, p. 7, 12. 2009. [PubMed: 19445663]

[15]. Reneman RS, PG Hoeks A, "Wall shear stress as measured in vivo: consequences for the design of the arterial system." Med. Biol. Engr. Comput, vol. 46, no. 5, pp. 499–507, 5 2008.

[16]. da Silveira LA, et al., "Arterial diameter of the celiac trunk and its branches: anatomical study." Acta Cirurgica Brasileira, vol. 24, no. 1, pp. 43–47, 1. 2009. [PubMed: 19169541]

[17]. Pries AR, et al., "Blood viscosity in tube flow: dependence on diameter and hematocrit." Am. J. Physiol.-Heart Circ. Physiol, vol. 263, no. 6, pp. H1770–H1778, 12. 1992.

[18]. Lowe GDO, "Blood rheology in vitro and in vivo." Bailliere's clinical haematology, vol. 1, no. 3, pp. 597–636, 9. 1987.

[19]. Eipel C, et al., "Regulation of hepatic blood flow: the hepatic arterial buffer response revisited." World J. gastroenterology: WJG, vol. 16, no. 48, p. 6046, 12. 2010.

[20]. Mancia G, et al., "Blood pressure and heart rate variabilities in normotensive and hypertensive human beings." Circulation research, vol. 53, no. 1, pp. 96–104, 7. 1983. [PubMed: 6861300]

[21]. Kretowski M, et al., "Fast algorithm for 3-D vascular tree modeling." Computer Methods and Programs in Biomedicine vol. 70, no. 2, pp. 129–136, 2. 2003. [PubMed: 12507789]

[22]. Carlisle KM, et al., "Estimation of total hepatic blood flow by duplex ultrasound." Gut, vol. 33, no. 1, pp. 92–97, 1. 1992. [PubMed: 1740284]

[23]. Segars WP, et al., “4D XCAT phantom for multimodality imaging research,” Medical Physics, vol. 37, no. 9, pp. 4902–4915, 9. 2010. [PubMed: 20964209]

[24]. Srihari SN, "Representation of three-dimensional digital images." ACM Computing Surveys (CSUR), vol. 13, no. 4, pp. 399–424, 12. 1981.

[25]. Zamir M, "Optimality principles in arterial branching." J. Theoretical Biol, vol. 62, no. 1, pp.227–251, 10. 1976.

[26]. Schreiner W, et al., "The influence of optimization target selection on the structure of arterial tree models generated by constrained constructive optimization." J. Gen. Physiol, vol. 106 no. 4, pp. 583–599, 10. 1995. [PubMed: 8576698]

[27]. Fung GSK et al., “Development of a model of the coronary arterial tree for the 4D XCAT phantom.” Phys. Med. Biol, vol. 56, no. 17, pp. 5651–5663, 9. 2011. [PubMed: 21828911]

[28]. Arts T, et al., "Propagation velocity and reflection of pressure waves in the canine coronary artery." Am. J. Physiol. -Heart Circ. Physiol, vol. 237, no. 4, pp. H469–H474, 10. 1979.

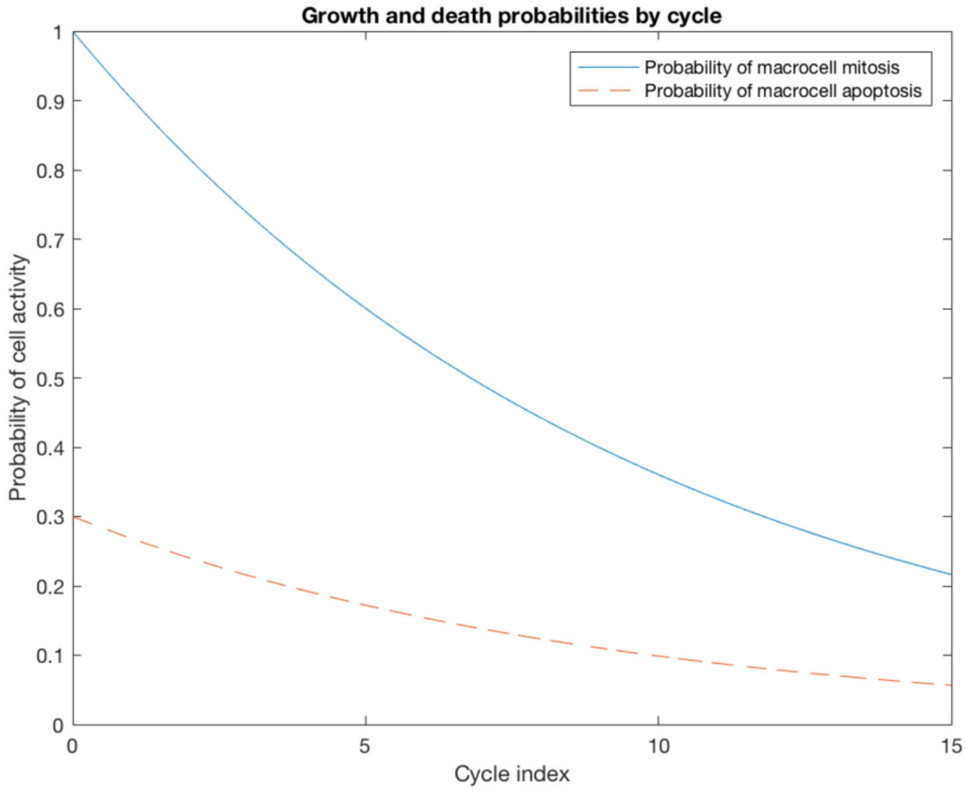

Fig. 1.

Probabilities of macrocell mitosis and apoptosis as a function of growth cycle number. Note that the probability of mitosis is always higher than that of apoptosis, leading to the shape eventually filling as the subcycles progress.

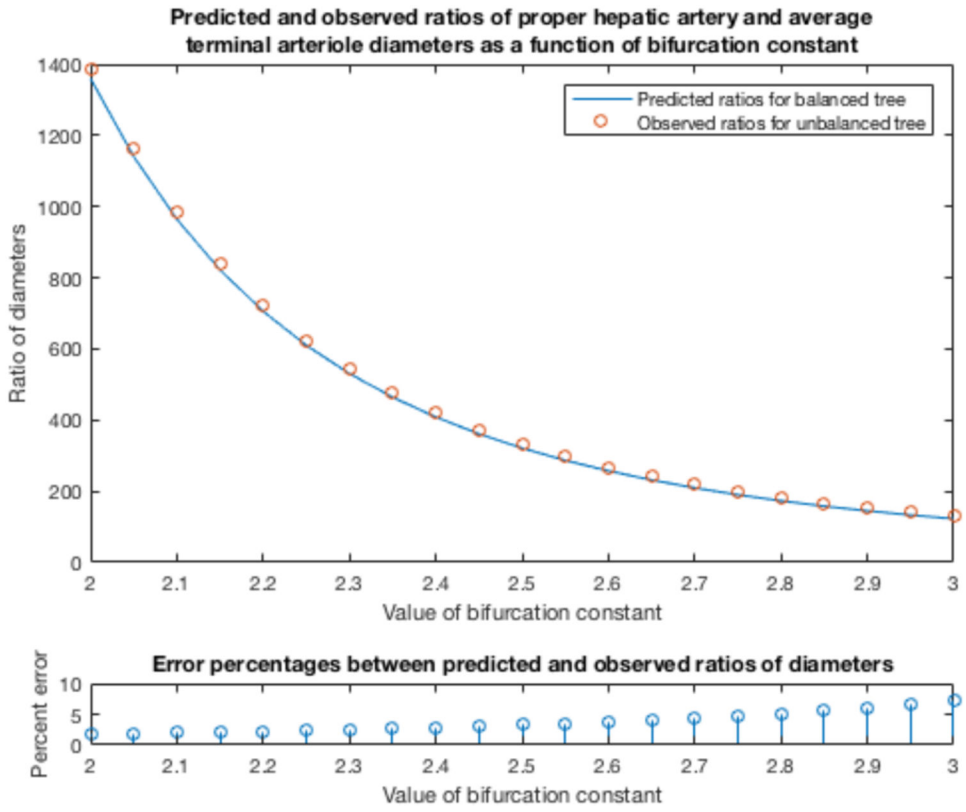

Fig. 2.

Ratio of PHA diameter over average THA diameter as a function of the bifurcation constant for a balanced binary tree and for several tree realizations built in this work. The percent difference between the ratio predicted using a balanced binary tree is less than 8%.

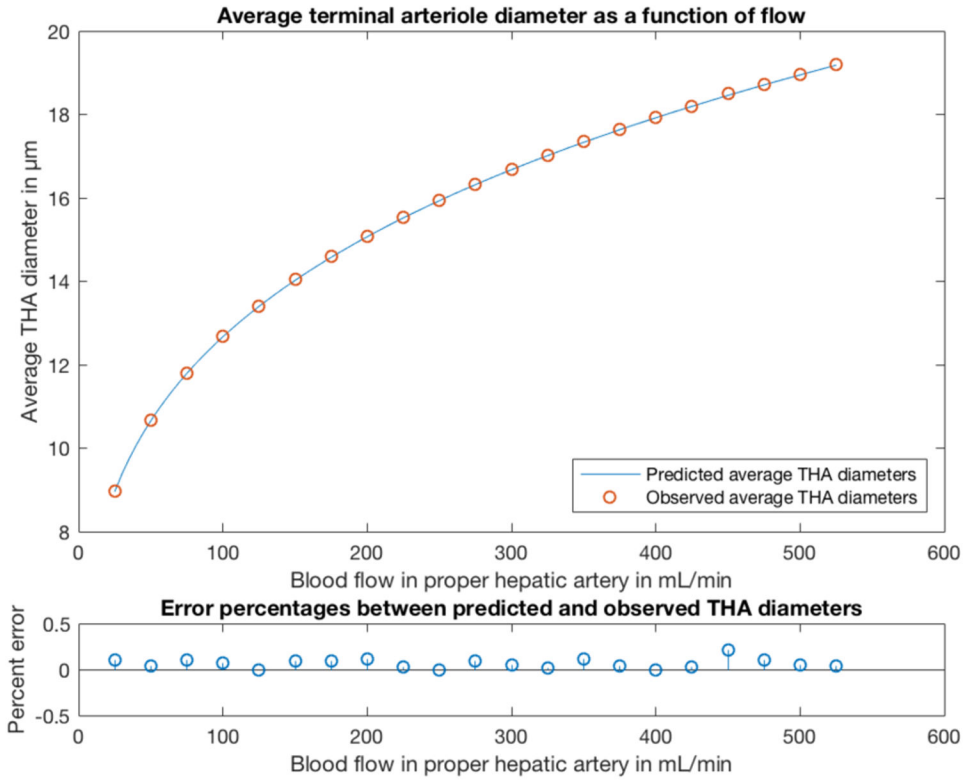

Fig. 3.

Average THA diameter as a function of the total hepatic arterial flow for trees generated with pressure difference 73 mmHg and $\gamma = 2.428$.

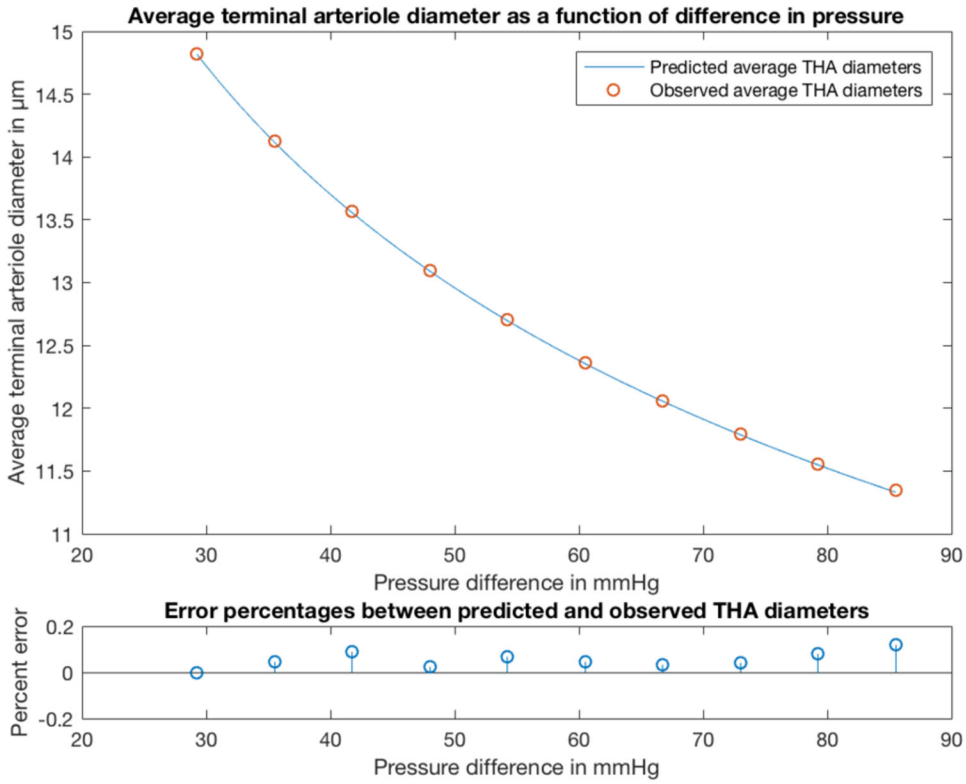

Fig. 4.

Average terminal vessel diameter as a function of the pressure difference between the PHA and THAs for 75 mL/min flow and $\gamma = 2.428$.

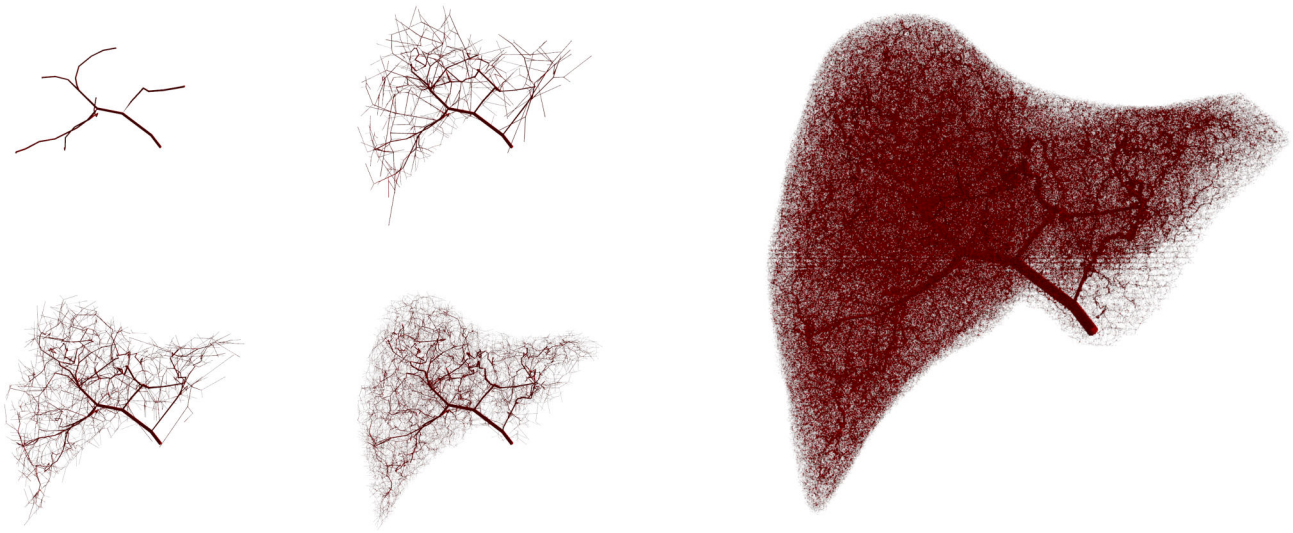

Fig. 5.

Tree growth from initial segmentation (top left), to cycle 4 (top center), cycle 8 (bottom left), cycle 12 (bottom center), and cycle 15 (right), which is the finished tree. Note that to aid visualization, the tree in earlier cycles has been scaled such that the liver shape occupies the same area of each image. Of interest is how the vessels taper in a manner comparable to true vessels. This allows embolic effects to be modeled in simulations of particle infusions.

Fig. 6.

A coronal slice from a simulated 120 Gy, whole-liver infusion convolved with a Gaussian filter at PET resolution. The texture is similar to that shown in Walrand *et al.* and indicates a heterogeneous distribution of spheres that may be sparing of normal tissue [9].